Iraqi Journal of Science, 2026, Vol. 67, No. 5, pp: 2994- 3004
DOI: 10.24996/ijs.2026.67.5.39

ISSN: 0067-2904

Simulation of an Antenna Array Factor Operating at the Wavelength of 0.21 m

Uday E. Jallod
Astronomy and Space Department, College of Science, University of Baghdad, Baghdad, Iraq

Received: 8/12/2024 Accepted: 29/ 5/2025 Published: 30/5/2026

Abstract

This study involves examining the antenna array factor using the MATLAB environment for three types of antenna arrays. These types are carried out to operate at the neutral hydrogen line emission of the wavelength of 0.21 m (this wavelength is very important in radio astronomy observations) with three configurations of antenna arrays. These configurations are a linear array, a planar array, and a circular array. The array factor is computed to include the linear array factor (*LAF*), planar array factor (*PAF*), and circular array factor (*CAF*), respectively. The array configuration is considered a crucial parameter that controls an array factor pattern, and it depends on the number of antenna elements with the distance between elements. Therefore, four values for antenna element numbers were chosen to achieve the best results for the array factor. These element numbers (*N*) are taken to be 3,5,7, and 10. Then, the antenna number is fixed at *N*=10, with different separation distances (*d*) given in terms of wavelength, and equal to 0.25λ, 0.5λ, 0.75λ, and λ. The results indicate that the (*LAF*) with *N*=10 and *d*=0.75λ yields the most optimal performance, characterized by a narrow main lobe and reduced side lobes, as compared with *PAF* and *CAF*.

Keywords: Astronomical antenna array, linear array factor, planar array factor, circular array factor, neutral hydrogen line emission.

محاكاة لمعامل صفيف الهوائيات مخصص للتردد 0.21 م

عدي عطيوي جلود
قسم الفلك والفضاء، كلية العلوم، جامعة بغداد، بغداد، العراق

الخلاصة

تتضمن الدراسة اختبار معامل نمط الاشعة لصفيف الهوائيات باستخدام بيئة الماتلاب لثلاثة انواع من صفيف الهوائيات. صممت هذه المعاملات لتعمل عند خط انبعاث الهيدروجين المتعادل بطول موجي 0.21 متر (هذا الطول الموجي مهم جدًا في الرصد الراديوي) بثلاثة توزيعات لصفيف الهوائيات. توزيعات صفيف الهوائيات الثلاثة هي مصفوفة خطية ومصفوفة مستوية ومصفوفة دائرية. وحسب معامل صفيف الهوائيات ليشمل معامل صفيف خطي، معامل صفيف مستوي، ومعامل صفيف دائري على التوالي. ولكون هندسة شكل المصفوفة يعد عامل حاسم يتحكم في معامل نمط الاشعة لمصفوفة الهوائيات، والذي بدوره يعتمد على عدد الهوائيات والمسافة بين الهوائيات. لذلك، تم اختيار أربع قيم لعدد الهوائيات لتحقيق أفضل النتائج لمعامل

*Email: uday.jallod@sc.uobaghdad.edu.iq

نمط الاشعة لمصفوفة الهوائيات. اخذت اعداد الهوائيات (N) لتكون 3 و5 و7 و10. بعد ذلك، تم تثبيت عدد الهوائيات عند $N = 10$، مع اخذ مسافات فصل مختلفة (d) بين الهوائيات معطاة بوحدة الطول الموجي وتساوي 0.25λ و0.5λ و0.75λ وλ. أظهرت نتائج الدراسة أن معامل المصفوفة الخطية مع $N = 10$ و $d = 0.75\lambda$ يعطي الاداء الامثل وذلك من خلال ضيق الفص الرئيسي وقلة الفصوص الجانبية لنمط معامل صفيف الهوائيات الخطية مقارنةً بمعامل صفيف الهوائيات المستوية والدائرية.

1. Introduction

Astronomical radio observations are required for the high resolution of observing systems because the observed radio waves are very weak. This means that a radio telescope should have a high directive gain to detect the weak radio waves that were emitted from a faraway celestial source [1]. The primary responsible part of a radio telescope, to obtain a high angular resolution is an antenna. An antenna is a vital component of small radio telescopes, capturing radio waves from space and transferring them to the receiver via a coaxial cable or waveguide [2]. Since a small single-element antenna has a poor resolution, due to its response (radiation pattern) has a wide main lobe. Therefore, multiple antennas are used to provide high angular resolution or sensitivity. These multiple identical antennas are utilized to form an array, which is called an antenna array [3]. This array is produced by individual elements with a certain amplitude and phase, to maximize a recorded signal [4].
The antenna arrays' geometry is classified into uniform and non-uniform arrays. A uniform array has an equal distance between elements. While a non-uniform array has different distances between element antennas [5]. These two classes can be configured as linear arrays, planar arrays, circular arrays, concentric circle arrays, hexagonal arrays, and so on [6]. The most common geometry is the first three types (i.e., linear, planar, and circular) of arrays. Antennas in a linear array have the simplest geometry and are arranged in a straight line either horizontally or vertically. The planar antenna array is distributed in the (x-y) plane as a matrix. This matrix could take the shape of a rectangular or square [7]. In a circular array, antennas are formed as a ring that is controlled by the radius of a circle [8].

The most important parameter of an antenna array is the radiation pattern. The total response of the array is the combination of the radiation pattern of multiple antennas instead of a single antenna, which is called the array factor. The other antenna characteristics depend on it, such as antenna directive gain, efficiency, effective area, and angular resolution. These antenna parameters that are generated by an array factor are enhanced by an enhancement of the radiation pattern [9]. Therefore, there are different variables are implemented to control the shape or the pattern of the array factor. These variables are the geometrical configuration or the shape of an array, the distance between array elements or array layout, and the amplitude and phase of a radiation pattern for each element [10,11].

An array can be employed in several fields, like communication networks, satellite communication, radar, and radio astrophysics observations [12]. During the past several years, the array factor has undergone a significant evolution in radio interferometry applications to construct high-resolution images of astronomical sources. Therefore, several large radio astronomical arrays were constructed, which were abbreviated as follows: In 1980, the construction of the Very Large Array (VLA) was completed, with a Y shape configuration. This array consists of 27 radio telescopes with a diameter of 30 m [13]. VLA is operated at four frequency bands (21 cm, 6 cm, 2 cm, and 1.3 cm) [14]. In 1998, the National Radio Astronomical Observatory (NRAO) built the Atacama Large Millimeter/Submillimeter Array (ALMA), located in Chile's desert. The ALMA position is in a dry site to allow atmospheric transmission of the wavelength (0.3 to 10) mm [15]. ALMA involves two arrays,

the first is 66 single elements, which have different diameters, where 50 elements have a diameter of 12 m, and the second is the Atacama Compact Array (ACA). ACA is constructed to obtain high imaging fidelity by a very short distance between them. ACA includes 4 elements with a diameter of 12 m, and 12 elements with a diameter of 7 m [16]. On the other hand, the Allen Telescope Array (ATA) represents a dramatic change. Since it has a large number of antennas of (350) elements with a diameter of 6 m, which are positioned at the Hat Creek Radio Observatory in northern California.

This number is sufficient to yield a radio image in a single field of 15000 independent pixels. ATA was started in 2001 and was completed in 2007. It includes a wide frequency range from 0.5 GHz to 10 GHz [17]. The largest project is the Square Kilometer Array (SKA) to build a next-generation radio telescope. The SKA consists of two phases, which are SKA1 and SKA2. These phases are achieved by 11 countries [18, 19]. One of the important goals of SKA is the imaging of the neutral hydrogen line emission.

This study aims to examine the array factor at the wavelength of 0.21 m. This array factor is simulated for three arrays with different configurations, numbers of elements, and distances between elements. The three array configurations include a linear array, a planar array, and a circular array. While the element numbers (N) are taken to be 3,5,7, and 10. Then, the antenna number is fixed at N=10, with different separation distances (d) given in terms of wavelength, and equal to 0.25λ, 0.5λ, 0.75λ, and λ. Consequently, the best array factor is multiplied by the radiation pattern of the small parabolic antenna; it is a generally weak antenna. Hence, the antenna array factor is used to improve the sensitivity of the antenna. The fundamental mathematical formulation that describes the three antenna array factors is given in Section Two. Section three gives the results and discussions of the three types of antenna array factors. Finally, the conclusions are drawn in Section Four.

2. Mathematical Formulation

An antenna array radiation pattern (P) can be given by [20]:

$$P(\theta,\phi) = F(\theta,\phi)AF(\theta,\phi) \quad (1)$$

Where, θ,ϕ are elevation and azimuth angles, F is a single antenna radiation pattern, and AF is an array factor, which can be defined as a mathematical description used to represent the radiation pattern of an array where all array elements are identical isotropic radiators [21]. It has different forms according to the geometry of an array. AF is studied for three antenna arrays, which are the linear array, planar array, and circular array, as listed below.

The basic form of a linear array factor (LAF) could be derived as [22]:

$$LAF = \sum_{n=1}^{N} I e^{jx_n\psi+\beta} \quad (a)$$

I is the amplitude of the element, $j = \sqrt{-1}$, $x_n = (n-1)d$, n = 1, 2,….N, N is the number of elements, d is the distance between elements, $\psi = kdsin\theta + \beta$, k is a wave number, and β is the phase difference of the received radio wave at each element.

Substituting x_n in Eq. (a), we get:

$$LAF = 1 + e^{j\psi+\beta} + e^{j2\psi+\beta} + \cdots + e^{j(N-1)\psi+\beta} \quad (b)$$

Multiplying both sides of Eq. (b) with $e^{j\psi}$ to obtain:

$$LAFe^{j\psi} = e^{j\psi} + e^{j2\psi+\beta} + \cdots + e^{j(N-1)\psi+\beta} + e^{jN\psi+\beta} \quad (c)$$

Subtract Eq. (a) form Eq. (c) yields,

$$LAFe^{j\psi} - LAF = e^{jN\psi} - 1 \quad (d)$$

or,

$$LAF = \frac{e^{jN\psi}-1}{e^{j\psi}-1} = \frac{e^{j\frac{N}{2}\psi}\left(e^{j\frac{N}{2}\psi}-e^{-j\frac{N}{2}\psi}\right)}{e^{j\frac{\psi}{2}}\left(e^{j\frac{\psi}{2}}-e^{-j\frac{\psi}{2}}\right)} = e^{j(\frac{N-1}{2})\psi}\frac{\sin\left(\frac{N}{2}\psi\right)}{\sin\left(\frac{\psi}{2}\right)} \quad \text{(e)}$$

Eq.(e) is reduced by ignoring the phase factor $e^{j(\frac{N-1}{2})\psi}$ due to this term is not important since the array output is combination of multiple antennas. Then Eq. (e) is divided by N to normalize the *LAF*. Normalization means that the maximum value of *LAF* becomes equal to unity. Consequently, the *LAF* can be given by [23]:

$$LAF = \frac{1}{N}\frac{\sin(\frac{N}{2}\psi)}{\sin(\frac{\psi}{2})} \quad (2)$$

A planar array shape is more complicated than a linear array, since the elements are arranged as a grid or a matrix. This matrix is either rectangular or square in shape. A planar array factor (*PAF*) could be derived in the same manner as *LAF*. *PAF* can be given as [24]:

$PAF = \sum_{m=1}^{M}\sum_{n=1}^{N} I_{mn} e^{j(d_m sin\theta cos\phi + d_n sin\theta cos\theta)}$ (3)

Where M and N are the width and length of the array, d_m and d_n are the distances along the width and length, respectively.

or *PAF* is written by [25]:

$$PAF = \left[\frac{1}{M}\frac{\sin(\frac{M}{2}\psi_x)}{\sin(\frac{\psi_x}{2})}\right]\left[\frac{1}{N}\frac{\sin(\frac{N}{2}\psi_y)}{\sin(\frac{\psi_y}{2})}\right] \quad (4)$$

Eq. (4) is equivalent to Eq. (3), where all elements have the same amplitude I=1.

Where, $\psi_x = kd_x sin\theta cos\phi + \beta_x$, and, $\psi_y = kd_y sin\theta sin\phi + \beta_y$. d_x, d_y is the distance separation between elements, and β_x, β_y is the phase difference of elements along x and y axes, respectively [26].

The simplest type of circular array has an equal distance with an identical amplitude and phase of elements. Then, a circular array factor (C*AF*) is given as [27, 28]:

$$CAF(\theta,\phi) = \sum_{n=1}^{N} I_n e^{jkr sin\theta\cos(\phi-\phi_n)+\beta_n} \quad (5)$$

r is the radius of a circular array, ϕ_n is an angular position of nth element, and could be written as [29]:

$\phi_n = \frac{2\pi n}{N}$, n=1,2,3…N, and β_n is the phase difference of the received radio wave at each element of the circular array.

3. Results and Discussions

Two-dimensional plots are generated to illustrate the key characteristics of the antenna array factors, allowing for a visual comparison of their performance. The array factor is simulated in an array of size (256×256) pixels according to Eqs. (2-5). These equations are generated at the wavelength of (λ= 0.21 m). The generated pattern of an array factor depends on the geometry of distribution, the number (*N*) of antennas, and the distance (*d*) between antennas. The types of antenna arrays analyzed in this study include linear, planar, and circular configurations. In the linear array, *N* values are chosen to be 3,5,7, and 10. While the distance (*d*) is assumed to be (d=0.25λ m, d =0.5λ m, d=0.75λ m, and d=1λ m). These changes are done to demonstrate the convenient antenna array to record the hydrogen line emission (0.21 m). The results of Eq. (2) with a zero phase difference (β=0) are displayed in Fig. 1.

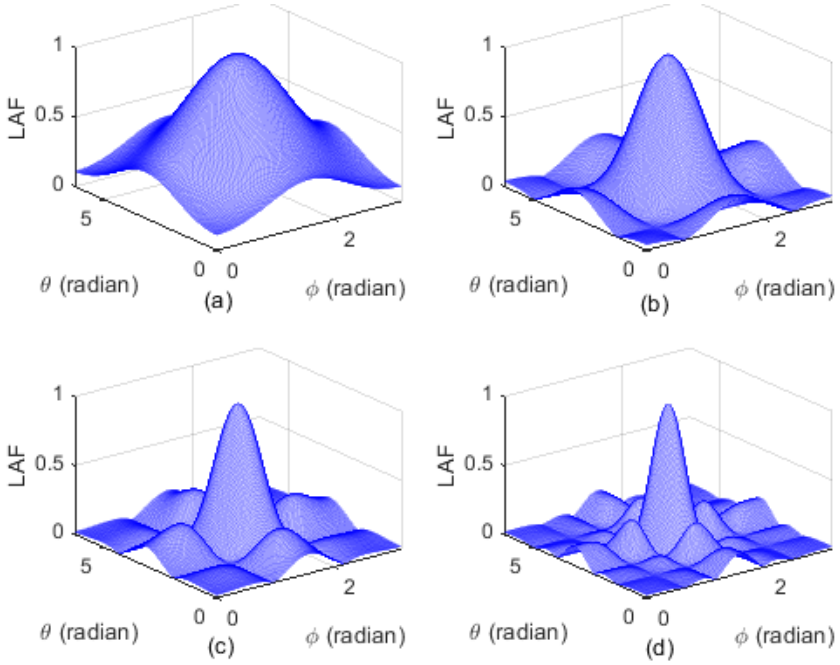

Figure 1: Two-dimensional plot of the linear array factor (*LAF*) using (d=0.25λ m) at different values of the number of elements (*N*). a- *N*=3, b- *N*= 5, c- *N*=7, d- *N*=10.

Fig. 1 demonstrates that increasing the number of antennas results in a narrower main lobe but also introduces additional side lobes, indicating a trade-off between sensitivity and directivity. In addition, the floor for each subplot becomes more convenient than the least number of antennas. It is clear that the *LAF* of (*N*=10) in Fig. 1 is the best result due to its narrow main lobe.

Another parameter that controls the array factor is the distance (*d*) between elements. The change of this parameter is computed with a fixed (*N*=10). This result is shown in Figure 2.

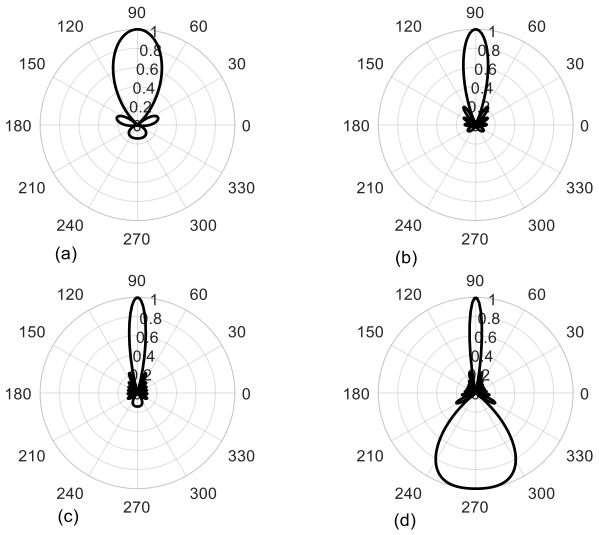

Figure 2: The polar plot of the linear array factor (*LAF*) for N=10 with different values of distance elements (*d*). a- *d*=0.25λ, b- *d*=0.5λ, c- *d*=0.75λ, d- *d*=λ.

Fig.2 displays acceptable results with some limitations. This limitation comes from increment values of *d*. At *d* equal to the observed wavelength, the *LAF* generates a back lobe. This back lobe is an undesired pattern in astronomical radio observations. The cross-section through Fig.2 is plotted as displayed in Fig.3.

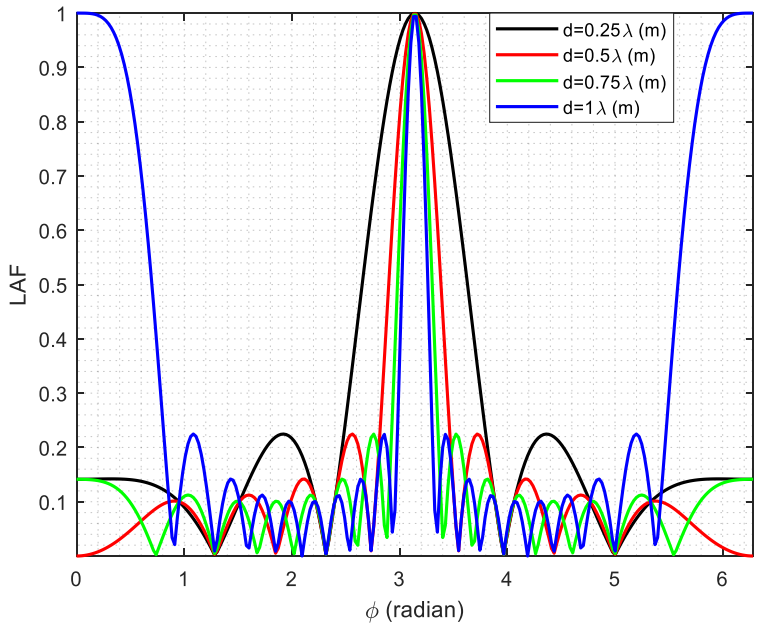

Figure 3: The cross-section of the linear array factor (*LAF*) as a function of azimuth (ϕ) for *N*=10 with different values of distance between elements (*d*).

It is clear that despite the large number of antenna elements (*N*=10), the small distance between elements is the worst result than the large distance, as demonstrated in Fig. 3. Therefore, *d* equal to 0.75λ gives the best result of the *LAF* since it has the narrow main lobe with the lowest level of the side lobes, as shown in the dashed line in Fig.3. At $d = \lambda$ the amplitude of back lobe of *LAF* is equal to the amplitude of the main lobe but in opposite direction, as displayed in the dotted line in Fig.3.

The planar array factor (*PAF*) is followed by the (*LAF*) in the same scenario. Then the result of Eq. (4) is demonstrated at the array size of ($N \times M = 2 \times 5$) and the different values of separation distance between elements) with zero phase difference, as illustrated in Fig.4.

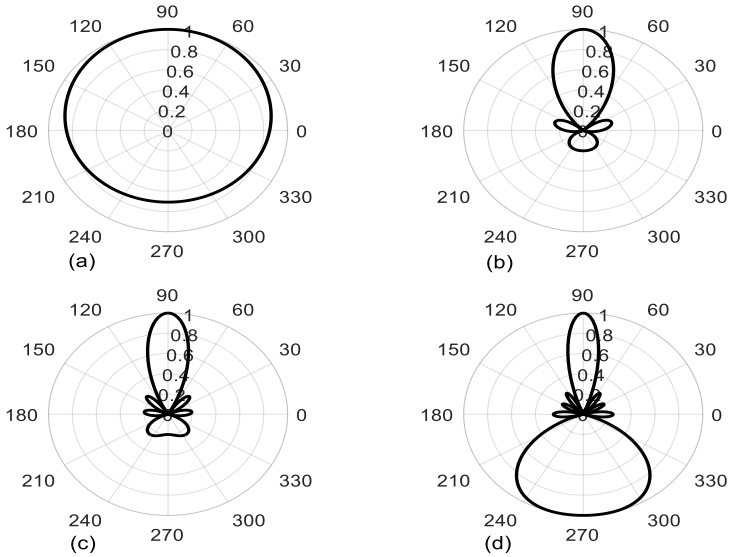

Figure 4: The polar plot of the planar array factor (*PAF*) for *N*×*M*=2×5 with different values of distance elements (*d*). a- $dx = dy = 0.25\lambda$, b- $dx = dy = 0.5\lambda$, c- $dx = dy = 0.75\lambda$, d- $dx = dy = \lambda$.

To verify the number of elements equal to 10, the number of rows N is set to 2, and the number of columns M is set to 5, and this setting gives a rectangular shape to the planar array. While a square shape of the planar array gives a better result than a rectangular one, it requires the array size equal to (N×M=5×5). This means that the number of elements is equal to 25 elements, and this number (25) is outside of our aim of study and prevents the comparison between the three types of arrays. Since the largest number of antennas, in this study, is 10.
To reveal more details, the central line is plotted through Fig.4, as shown in Figure 5.

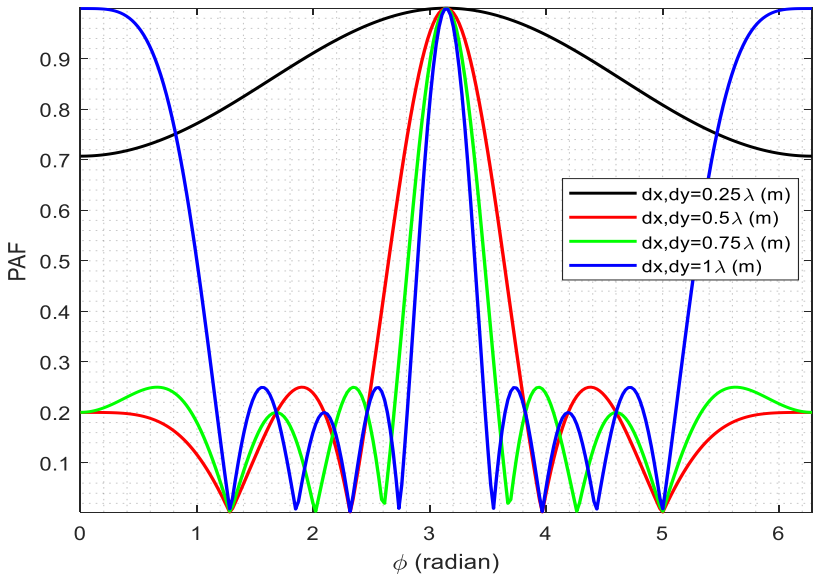

Figure 5: The planar array factor (*PAF*) as a function of azimuth (ϕ) for N×M=2×5 with different values of distance between elements (*dx* and *dy*).

Fig.5 shows the weakness of *PAF* obtained at the smallest distance between the elements (i.e. $dx = dy = 0.25\lambda$), which has a wider main lobe and approximately a third of the amplitude of the pattern than the others. While at the largest distance between elements ($dx = dy = \lambda$) it has the narrowest main lobe, but it has a big back lobe. Therefore, if these two results are excluded, then the acceptable results are obtained at ($dx = dy = 0.5\lambda$ or $dx = dy = 0.75\lambda$), but the best result is obtained at ($dx = dy = 0.75\lambda$) since is the narrow main lobe with a low level of side lobes, as illustrated in the dashed line in Fig. 5.

The circular array factor (*CAF*) is computed according to Eq. (5), and found the crucial parameter that controls the *CAF* the radius (r) of the circular array. This radius can be estimated using the formula (r=N *d). This formula means that the radius is determined by the number of elements and the separation distance between antenna elements. So, the *CAF* is computed in the same way that computed the *LAF* and *PAF,* respectively. This means that the best number of elements is found to be (N = 10) at the separation distance between elements ($d = 0.25\lambda$). Then the number of elements is fixed at (N = 10) with four values of (d), which started from ($d = 0.25\lambda$ to $d = \lambda$). All these changes are carried out with a zero phase difference ($\beta_n = 0$). The results are illustrated in Fig.6.

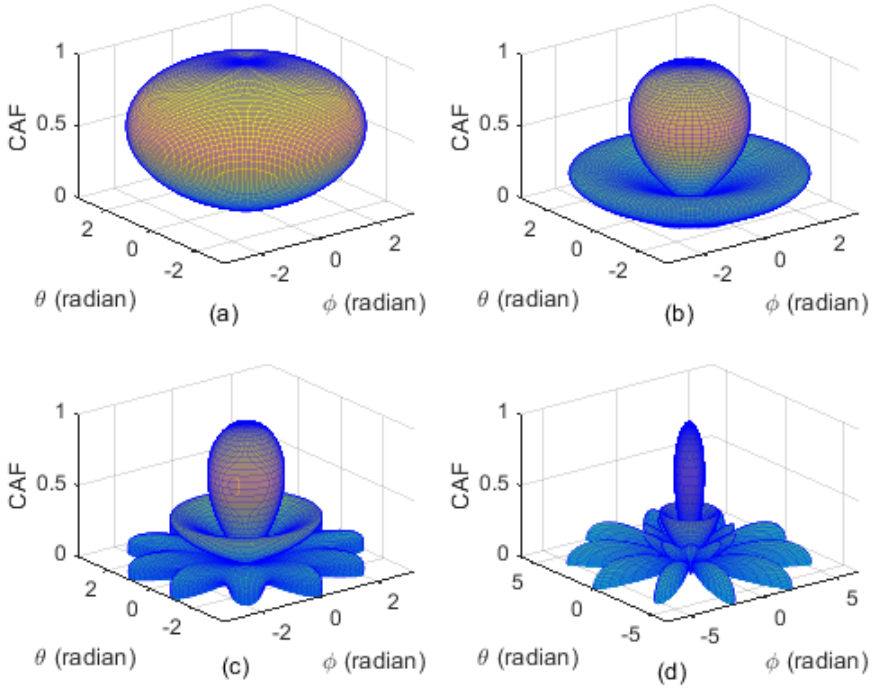

Figure 6: Two-dimensional plot of the circular array factor (*CAF*) of fixed (*N*=10) with different values of radius (*r*). a- *r*=*N**0.25λ, b- *r* = *N* *0.5λ, c- *r* = *N* *0.75λ, d- *r* = *N* *λ.

It should be noted here that the largest radius gives the best result of *CAF*, because it has a narrow main lobe, but recognized side lobes, as shown in Fig.6-(d).
To prove which array configuration is the best, the array factor for three arrays (linear, planar, and circular) is plotted as displayed in Figure 7.

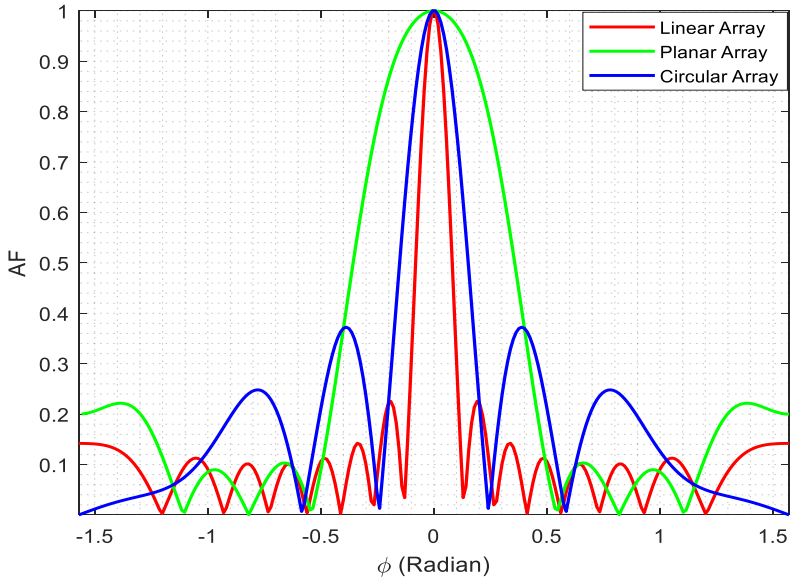

Figure 7: The central line of the array factor (*AF*) as a function of azimuth (ϕ) for *N*=10.
Fig.7 shows that the *LAF* and the *CAF* are very close together in the main lobe, but the *CAF* has a larger side lobe than the *LAF*. In addition, the *LAF* has a good result compared to the *PAF* and *CAF*. This good result of the *LAF* comes from three reasons. The first reason is that the *LAF* does not need a large number of antennas, as compared with others. The second is that the *PAF* needs to have 25 elements or more, i.e., array size at least equal to [*N*×*M*=5×5].

This number gives a square shape to the planar array and leads to narrowing the large main lobe. The third reason is that the *CAF* needs more rings to overcome the large side lobes.
Now, Eq. (1) can be simulated by generating a radiation pattern (*F*) of a small parabolic antenna with a diameter of 1 m. *F* is generated according to the following Eq. (6) [30]:

$$F(\theta,\phi) = \left[\frac{2J_1\left(\frac{\pi UD}{\lambda}\right)}{\left(\frac{\pi UD}{\lambda}\right)}\right] \quad (6)$$

Where J_1 is the first order of the Bessel function, U =sin(θ), and D is the diameter of the parabolic reflector antenna.
Then Eq. (6) is multiplied by *LAF* (Eq. (2)) to obtain the array radiation pattern (*P*), as given in Eq. (1). The result of Eq. (1) is demonstrated in Fig.8.

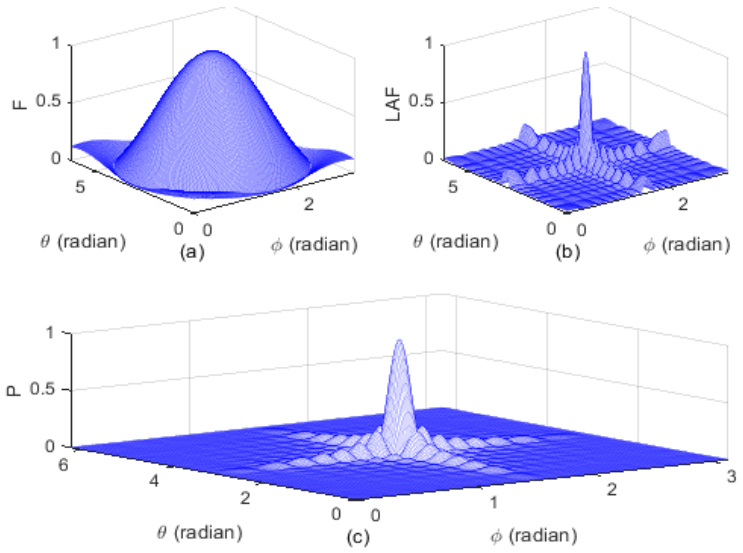

Figure 8: Two-dimensional plot of: (a) The radiation pattern of the parabolic antenna of diameter (*D* = 1m), (b) The linear array factor (*LAF*) for *N*=10 with d=0.75λ, and (c) The result of multiplication of (a) and (b).

It should be remembered that the radiation pattern of the parabolic reflector antenna is clearly enhanced by multiplication of the *LAF*, as shown in Fig.8(c). This enhancement involves two issues: the first is to narrow the main lobe by a large factor, and the second is the attenuation of the side lobes. This is considered more convenient than the before process of multiplication with the *LAF*. Consequently, it leads to precise radio observations by increasing the pointing of the radio telescope.

4. Conclusions

The small parabolic reflector antenna, particularly one with a diameter of D = 1 m, is easier to design and requires lower material costs compared to larger radio telescope antennas. However, the antenna radiation pattern of the small radio telescope is wider than the pattern of large radio telescope antennas. The wider radiation pattern of small telescope antennas typically results in lower gain and sensitivity, as well as poorer angular resolution, under standard operating conditions. So, the necessity of good observation requires increasing the telescope antenna gain, sensitivity, and resolving power. This is done by designing an antenna array instead of a single large telescope antenna. The antenna array factor is a critical parameter that controls the overall performance of the array. This array factor is simulated at a wavelength of 0.21 m. The array factor is strongly dependent on three parameters: the shape of the array, the number of elements, and the distance between

elements. Therefore, the array factor is computed for three arrays with different shapes. These types are the linear array, planar array, and circular array. Each array factor of three antenna arrays is simulated with four values of the antenna number and four values of the distance between antennas. These changes are taken to obtain acceptable results for the antenna array factor. The results showed that the best array factor is obtained via the linear array by setting the number of elements (N =10) and distance between elements (d = 0.75λ). In contrast, the planar and circular arrays need more antennas to fill the geometry of their shapes to give the same result as compared by the linear array. Therefore, the linear array result is found to have narrowed the main lobe with low side lobe levels (see Fig. 8). This narrow main lobe, achieved by the optimal array configuration, indicates improved directive gain, enhanced sensitivity, and better angular resolution compared to the traditional single-element antenna. This result is expected to enhance the quality of radio observations.

5. Disclosure and conflict of interest

"Conflict of Interest: The author declares that he has no conflicts of interest."

References

[1] G. Gancio, C. O. Lousto, L. Combi, S. del Palacio, F. G. Lopez Armengo, J. A. Combi, F. Garcia, "Upgraded antennas for pulsar observations in the Argentine Institute of Radio astronomy", *A&A*, vol. 633, A84, pp.1-12, 2020.

[2] A. A. Hatem, and A. I. Ali, "Design and implementation of Slotted Waveguide Antennas with Low Sidelobe Level in X-band for High Power Application", *5th IUGRC International Undergraduate Research Conference*, Cairo, Egypt, July 29th – Aug 1st, 2021.

[3] Yihong Qi, Wei Yu, "Unified Antenna Temperature", *IEEE Transactions on Electromagnetic Compatibility*, pp:1-7, 2016.

[4] E. Juarez , M. A. Panduro, A. Reyna, D. H. Covarrubias, A. Mendez, and E. Murillo, "Design of Concentric Ring Antenna Arrays Based on Subarrays to Simplify the Feeding System", *Symmetry* vol. 12, pp.1-15,2020 doi:10.3390/sym12060970.

[5] H. LIU, J. GAO, F. HE, and Q. LIU, "Curtain Antenna Array Simulation Research Based on MATLAB", *Sensors & Transducers*, vol. 163, Issue 1, pp. 9-14, 2014.

[6] A. A. Qasim, and A.H. Sallomi, "Design and Analysis of Phased Array System by MATLAB Toolbox", *Al-Kitab Journal for Pure Science*, vol.4 (1), pp:52-65, 2020.

[7] D . Kalaiarasi, M.R. Jebarani, "Embedded Pattern Analysis of Planar Phased Array Antenna for X Band Communication Systems", *Journal of Theoretical and Applied Information Technology*, vol. 102, no.9, pp. 4050-4060, 2024.

[8] N. Mukit, M. R. Islam, M. H. Habaebi, A. H. Alam, K. Abdullah, N. F.Abdul Malek, R. Nibir, N. M. Adnan, and E. Osman, "Designing large-scale antenna array using sub-array", *Bulletin of Electrical Engineering and Informatics*, vol. 8, no. 3, pp. 906-915, 2019.

[9] H. A. Abdulsada, and H. Razzaq, "50x50 Elements Phased Array Antenna using MATLAB and CST", *International Journal for Research in Applied Science & Engineering Technology (IJRASET)*, vol. 7 Issue III, pp: 196-200, 2019.

[10] C. Kolitsidas, *Next Generation Wideband Antenna Arrays for Communications and Radio Astrophysics*, Ph. D thesis in Electrical Engineering School of Electrical Engineering, KTH Royal Institute of Technology, pp:8-10, 2017.

[11] M. A. McCulloch, M. D. Cruze, K. Grainge, M. Keith and S. Melhuish, "An *S* -band cryogenic phased array feed for radio astronomy", *Royal Astronomical Society*, vol. 2, pp. 432-440, 2023.

[12] B. E. Cohanim and J. N. Hewitt, "The Design of Radio Telescope Array Configurations Using Multiobjective Optimization: Imaging Performance Versus Cable Length", *The Astrophysical Journal Supplement Series*, vol. 154, pp.705–719, 2004.

[13] S. Kiehbadroudinezhad, J. Bousquet, M. Cada, C. I. Short, A. Shahabi, S. Kiehbadroudinezhad, "Expansion of a *Y*-Shaped Antenna Array and Optimization of the Future Antenna Array in Malaysia for Astronomical Applications", *Journal of Modern Physics*, vol. 10, pp. 888-908, 2019.

[14] K. I. Kellermann, E. N. Bouton, S. S. Brandt, *Open Skies*, Springer, p.319, 2021.
[15] A. Wootten and A. R. Thompson, "The Atacama Large Millimeter/submillimeter Array", *Proceedings of the IEEE*, vol. 97, Issue 8, pp:1463 – 1471, 2009.
[16] S. Iguchi, K. I. Morita, M. Sugimoto, B. V. Vilaro, M. Saito, T. Hasegawa, R. Kawabe, K. Tatematsu, S. Sakamoto, H. Kiuchi, S. K. Okumura, G. Kosugi, J. Inatani, S. Takakuwa, D. Iono, T. Kamazaki, R. Ogasawara, and M. Ishiguro, "The Atacama Compact Array (ACA)", *PASJ: Publ. Astron. Soc. Japan*, vol. 61, pp.1-12, 2009.
[17] M. Atemkeng, P. Okouma, E. Maina, R. Ianjamasimanana, and S. Zambou, "Radio Astronomical Antennas in the Central African Region to Improve the Sampling Function of the VLBI Network in the SKA Era", *Sensors*, vol. 22, pp. 1-16, 2022.
[18] A. Keerthipriyasatish, A. Sathyamurthy, T. Prabu, B. S. Girish1, K.S. Srivani, and S. K. Sethi, "Antennas for Low-frequency Radio Telescope of SKA", *J. Astrophys. Astr*., vol. 44, no.43, pp.1-14, 2023.
[19] W. P. du Plessis, "Efficient Computation of Array Factor and Sidelobe Level (SLL) of Linear Arrays", *IEEE Antennas & Propagation Magazine*, vol. 58, no. 6, pp.102-114, 2016.
[20] G. Karunakar, and S. Sairam and D. Reshma, "Analysis of Linear and Planar Antenna Arrays", *International Journal of Science Engineering and Advance Technology, IJSEAT*, vol.3, Issue 4, pp.151-155, 2015.
[21] M. H. Agha, M. A.S. Al-Adwany, O. Bayat , H. T. Hamdoon, "Optimization of Antenna Array Pattern for Uniformly Excited Rectangular Array via a Thinning Method", *Journal of King Saud University – Engineering Sciences*, vol. 34, pp.544–561, 2022.
[22] S. Ogurtsov, D. Caratelli, and Z. Song, "A Review of Synthesis Techniques for Phased Antenna Arrays in Wireless Communications and Remote Sensing", *International Journal of Antennas and Propagation*, vol. 2021, pp.1-20, 2021.
[23] E. Yaacoub, M. Al-Husseini, A. Chehab, A. E. Hajj, and K. Y. Kabalan, "Hybrid Linear and Circular Antenna Arrays", *Iranian Journal of Electrical and Computer Engineering*, vol. 6, no.1, pp. 48-54, 2007.
[24] S. Chakraborty, S. Thyadi, P. Kumar, L. R Sahana, and K. Meghana, "Adaptive Beam Synthesis for Phased Array Antenna", *International Journal of Engineering Trends and Technology (IJETT)*, vol. 61, no.1, pp.449-453, 2013.
[25] A. Vesa, F. Alexa, and H. Balta, "Comparisons between 2D and 3D Uniform Array Antennas", *Proceedings of the Federated Conference on Computer Science and Information Systems*, vol. 67, Issu.5, pp. 144–148, 2019.
[26] K. S. Ahmad, M. Z. Aziz, "Pattern Reconfigurable Planar Antenna Array Based on Two Circular Defected Ground Structure", *Przegląd Elektrotechniczny*, vol. 97, pp. 52-55, 2021.
[27] A. H. Aboud, and M. Z. Mohammed, "Sidelobes Reduction Method in Circular Antenna Array", *International Journal of Engineering and Innovative Technology (IJEIT)*, vol. 7, Issue 9, pp: 1-5, 2018.
[28] V. Mittal, K. P. Sharma, N. Thangarasu, U. Sarat, A. O. Hourani, and R. Salgotra, "Synthesis of Circular Antenna Arrays for Achieving Lower Side Lobe Level and Higher Directivity using Hybrid Optimization Algorithm", *Algorithms Journal*, vol. 17, no. 256, pp.1-19, 2024.
[29] V. K. Tulasi, K. R. Kumar, V. L. Rao, "Design of Linear and Circular Antenna Array for Side Lobe Reduction Using the Method Moth Flame Optimization Algorithm", *International Journal of Scientific Engineering and Applied Science (IJSEAS)*, vol. 6, Issue 9, pp.78-90,2020.
[30] U. E. Jallod, H. S. Mahdi, and K. M. Abood, "Simulation of Small Radio Telescope Antenna Parameters at Frequency of 1.42 GHz", *Iraqi Journal of Physics*, vol. 20, no.1, pp. 37-47, 2022.